文章编号：1001－9014(2018)02－0154－09

DOI:10.11972/j.issn.1001－9014.2018.02.005

# Construction and application effects of normalized shaded vegetation index (NSVI)

XU Zhang-Hua[1,2,3,4], LIN Lu[1], WANG Qian-Feng[1*], HUANG Xu-Ying[1], LIU Jian[4], YU Kun-Yong[4], CHEN Chong-Cheng[2]

(1. College of Environment and Resources, Fuzhou University, Fuzhou 350116, China;
2. Key Lab of Spatial Data Mining & Information Sharing, Ministry of Education, Fuzhou 350116, China;
3. Fujian Provincial Key Laboratory of Remote Sensing of Soil Erosion and Disaster Protection, Fuzhou 350116, China;
4. Fujian Provincial Key Laboratory of Resources and Environment Monitoring & Sustainable Management and Utilization, Sanming 365004, China)

**Abstract**: The spectral features and differences in bright vegetation area, shaded vegetation area and water area were investigated by the experimental data from four medium resolution remote sensing images of ALOS AVNIR-2, CBERS-02B CCD, HJ1A-CCD2 and Landsat 7 ETM. Based on the near-infrared band and normalized difference vegetation Index (NDVI), Normalized Shaded Vegetation Index (NSVI) was constructed and the enhancements of spectral differences and classification effect were also evaluated. The results show that NSVI has increased the relative diferences of the spectra in bright vegetation area, shaded vegetation area and water area, and reduced probability of misapplication for the spectral data. The NSVI threshold method was employed to classify the four experimental images. The overall accuracy is over 97%, and the overall Kappa coefficient is above 0.96. The detection accuracy of the shaded vegetation area is over 94% and the Kappa coefficient is also higher than 0.96. By using radiation differences of the near-infrared band between the ground objects, NSVI can solve the problem that NDVI can only partially weaken the topographic effect and enlarge the spectral differences among the ground objects. NSVI enhances the validity of the ground objects especially in the shadow detection and avoids the "saturation" problem of NDVI. It can provide a new solution to remove the shadow in remote sensing images.

**Key words**: normalized shaded vegetation index(NSVI), bright vegetation area, shaded vegetation area, water area, shadow detection

**PACS**: 42.68.Wt, 02.70.Hm

# 归一化阴影植被指数 NSVI 的构建及其应用效果

许章华[1,2,3,4], 林 璐[1], 王前锋[1*], 黄旭影[1], 刘 健[4], 余坤勇[4], 陈崇成[2]

(1. 福州大学 环境与资源学院,福建 福州 350116;
2. 空间数据挖掘与信息共享教育部重点实验室,福建 福州 350116
3. 福建省水土流失遥感监测评估与灾害防治重点实验室,福建 福州 350116;
4. 福建省资源环境监测与可持续经营利用重点实验室,福建 三明 365004)

**摘要**:以 ALOS AVNIR-2、CBERS-02B CCD、HJ1A-CCD2、Landsat 7 ETM 四幅中分辨率遥感影像为试验数据,分析明亮区植被、阴影区植被与水体区的光谱特征与差异,基于近红外波段与归一化植被指数 NDVI,构建归一化阴影植被指数 NSVI,并评价其光谱差异增强及分类效果.结果表明,NSVI 大幅扩大了明亮区植被、阴影区植被、水体区间的光谱相对差异,降低光谱混淆概率;利用 NSVI 阈值法对四幅试验影像进行分类,总精度均大于97%,总 Kappa 在0.96以上,且阴影区植被的检测精度均在94%以上,总 Kappa 系数亦高于0.96.该指

**Received date**: 2017-09-16, **revised date**: 2017-12-20 **收稿日期**:2017-09-16, **修回日期**:2017-12-20

**Foundation items**: Supported by National Natural Science Foundation of China (41501361, 41401385, 30871965), Open Fund of Fujian Provincial Key Laboratory of Resources and Environment Monitoring & Sustainable Management and Utilization (ZD1403), Fujian Natural Science Foundation (2016J01188), and Scientific Research Foundation of Fuzhou University (XRC1345)

**Biography**: XU Zhang-Hua(1985-), male, Fuqing China. Associate professor, Ph. D. Research fields involve resource and environment remote sensing, urban and rural planning, and the application of GIS. E-mail: fafuxzh@163.com

* **Corresponding author**: E-mail: wangqianfeng@fzu.edu.cn

数利用地物在近红外波段的辐射差异,解决 NDVI 只能部分削弱地形影响的问题,扩大地物间的光谱差异,从而提升地物尤其是阴影检测的有效性,且不存在 NDVI"易饱和"问题,可为遥感影像阴影去除提供一种新的解决方案.

**关　键　词**:归一化阴影植被指数;明亮区植被;阴影区植被;水体区;阴影检测

**中图分类号**:TP75,O433.4　　**文献标识码**:A

## Introduction

Due to the mixed effects of solar incident angle, satellite pendulum, objects height and topography, there are differences in spectral response to the same objects, namely "the same object has different spectra". When illuminated area is enlarging, it will form bright area caused by high brightness; when light is blocked, it will lead to shaded area. Thus, the remote sensing images display two levels of brightness and shadow which make more strong sense of three-dimension. Loss of information on remote sensing images in shaded area seriously interferes with the accurate object recognition and the construction of quantitative algorithm[1-3]. With persistently improved spatial resolution of remote sensing images, the interference of shadow is also intensified. It has become a consensus to urgently detect and eliminate the influence of shadow[4-6]. The previous studies on shadow removal of remote sensing images are mostly based on the shadows of civic architectures and the data sources with high spatial resolution. For instance, Li *et al.* [7] came up with a method for automatic shadow detection and shadow removal, including shadow stimulation, ray tracing, integrated shadow detection, shadow removal and other procedures. Yang *et al.* [8] presented an automatic property-based approach for shadow removal of color image. Yamazaki *et al.* [9] analyzed the radiation effects of architectural shadows of QuickBird in which the threshold method was used to extract shadows and the spectral relationship model of the same object in bright area and shaded area was constructed respectively which was conducive to spectral correction. Zigh *et al.* [10] proposed a method in automatic shadow detection and shadow removal by the virtue of high resolution images of dense urban area which contains shadow extraction with property based method and stereo matching. Su *et al.* [11] proposed a new algorithm for the shadow problem of panchromatic spectral image with high resolution in urban area. Combined with the application of a bi-model histogram splitting method and image matting technique, the algorithm can realize automatic detection of shadows and remove shadows by the virtue of spatial adaptive non-local sparse shadow removal method. Obviously, shadow detection is an indispensable and fundamental step to remove the shadow of remote sensing images and its effectiveness is an important guarantee[6,12-14]. However, there are confusing problems between images of shadow and water and other objects[15], namely the phenomena of "the different objects are in the same spectrum".

The shadow detection procedure should be further investigated by enlarging the spectral difference between different objects, especially the shaded area and other objects, as well as effectively reducing the spectral confusion probability of different objects. In addition, the study brings forth some new ideas on data source and survey regions with medium resolution remote sensing images mainly cover non-urban areas, and enhances spectral recognition of ground objects through the calculation of bands and the construction of new index model.

## 1　Experimental data

To analyze the construction principles and application effects of Normalized Shaded Vegetation Index (*NSVI*), four multi-spectral images were derived from Japan ALOS AVNIR-2 (Level 1B2), China CBERS 02B-CCD (Level 2), China HJ1A-CCD2 (Level 2) and USA Landsat 7 ETM. The transiting time and track number of its corresponding satellite is respectively: November 8, 2010, 25513/3100; November 20, 2009, 371/72; May 25, 2010 449/88; March 10, 2003, 135/41. The obtained images were not involved with preprocessing steps, such as radiometric correction, geometric correction, orthorectification and so on. The multi-spectral bands design parameters of four remote sensing images are as shown in Table 1. To improve the efficiency of the experiment, small parts of regions were masked from the four remote sensing images respectively as the experimental data. The experimental regions are located in the south of China, with large topographic relief and high vegetation coverage (Fig. 1). The experimental data of ALOS AVNIR-2 is 1012 rows × 571 columns, collected in Zhangpu County of Fujian Province; the data of

**Table 1　Multi-spectral bands design of four remote sensing images**
**表 1　四种遥感影像多光谱波段设计**

| | ALOS AVNIR-2 | CBERS-02B CCD | HJ1A-CCD2 | Landsat 7 ETM |
|---|---|---|---|---|
| Blue band | 0.42 ~ 0.50 μm | 0.45 ~ 0.52 μm | 0.43 ~ 0.52 μm | 0.45 ~ 0.52 μm |
| Green band | 0.52 ~ 0.60 μm | 0.52 ~ 0.59 μm | 0.52 ~ 0.60 μm | 0.52 ~ 0.60 μm |
| Red band | 0.61 ~ 0.69 μm | 0.63 ~ 0.69 μm | 0.63 ~ 0.69 μm | 0.63 ~ 0.69 μm |
| Near-infrared band | 0.76 ~ 0.89 μm | 0.77 ~ 0.89 μm | 0.76 ~ 0.90 μm | 0.76 ~ 0.90 μm |
| Short-wave infrared band | – | – | – | 1.55 ~ 1.75 μm (Band 5)<br>2.08 ~ 2.35 μm (Band 7) |
| Pixel size | 10 m | 19.5 m | 30 m | 30 m |

CBERS 02B-CCD is 520 rows × 294 columns, collected in Ganzhou City of Jiangxi Province; the data of HJ1A-CCD2 is 964 rows × 525 columns, collected in the central area of Taiwan Province; the data of Landsat 7 ETM is 631 rows × 357 columns, collected in southern Tibet. By observing the remote sensing images, it can be seen apparently that the vegetation is the main object in the image and there are obvious bright and shaded layers in the vegetation area. The phenomenon of "the same object has different spectra" is common. Therefore, it was selected as experimental data to test the validity of the constructed index.

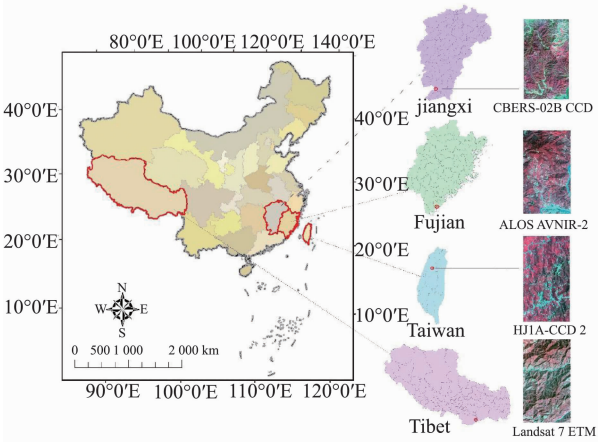


Fig. 1 Experimental remote sensing images (RGB: NIR, R, G)

图 1 试验影像(RGB:近红外波段、红光波段、绿光波段)

## 2 Principle and method for construction of NSVI

### 2.1 Analysis on spectral features of remote sensing images

The experimental images contain rich information of vegetation, followed by water area and a small part of lands for residence and transportation. Through the construction of NSVI which can enlarge the spectral differences among bright vegetation area, shaded vegetation area and water area, the study focuses on the spectral features of the above three types of objects and other objects are ignored. In this study, the grey information of the original pixels was kept and was not stretched and the data type was unsigned 8-bit with grey value ranges [0, 255]. NDVI is one of the most widely used vegetation indices in vegetation extraction[15-17]. Therefore, the NDVIs of each remote sensing image in the experimental area except the original bands were normalized and the value belonged to the range [0, 1]. 90 coordinates were generated in each remote sensing image and distributed uniformly in the bright vegetation area, shaded vegetation area and water area which helped to read DN value and NDVI value of each band by providing the coordinate information.

There are differences in features between the original DN and actual reflectivity before radiometric correction, atmospheric correction and other preprocessing. It is mainly manifested in the vegetation area where the spectral value of blue band is higher than that of green band, unlike the small peak of reflection which is formed by the green band. Apart from that the spectral value of red band is a little higher than that of the green band for data of CBERS-02B CCD, in the other three remote sensing images, the vegetation DN value of visible bands decreases with the increase of wavelength. Nevertheless, it can sum up several important features (Fig. 2): (1) In the near-infrared band, the vegetation spectral value is much greater than that of the visible bands and rises steeply which correspond to the vegetation spectral features. It shows that the rich information of the near-infrared band is a significant feature in extracting vegetation information. (2) Whether in bright vegetation area or in shaded vegetation area, there are similar features in the spectral curve of the region between the visible to the near-infrared bands. The value of shaded vegetation area is lower than that of the bright vegetation area with different descent degree which indicates that more information of shaded vegetation area is lost. This adds the difficulty for its precise extraction. (3) In the case of taking only spectrum average into consideration, the spectral response curves of bright vegetation area and shaded vegetation area do not cross and their differences in the near-infrared band are much greater than that in the visible region. However, if all the DN values of sample points are taken into account, it will increase the confusion in these two different vegetation areas. (4) Compared with the vegetation, it is more complicated to measure spectral response of water by the sensors which are related to the types of water including the quality of water, hydrology and other conditions[18-21]. In four experimental areas, the spectral response curves of water area and vegetation areas are across and there is less difference between water area and shaded vegetation area than bright vegetation area. This shows that the differences among the bright vegetation area, shaded vegetation area and water area in the near-infrared band are greater than that of the visible bands, but there still is a common phenomenon of confusing spectra.

NDVI is considered as the best indicator for the ecological status and the coverage of vegetation, and it is also one of the most widely used remote sensing indices which can remove the effects of sun elevation angle, satellite observation angle, topography, cloud shadows and other changes in radiation which are related to atmospheric conditions. However, NDVI is not sensitive enough to assess the high vegetation coverage areas and is easy to be saturated[22-26]. Normally, NDVI is limited to [0, 1]; in general, the negative value represents that what covers the ground is cloud, water, snow, etc; 0 represents the existence of rock or bare soil; the positive value indicates vegetation cover. In other words, by virtue of positive values and negative values, NDVI can serve as an empirical criterion to distinguish vegetation cover from other objects covers. In this study, the range of NDVI is [0, 1] and it can obtain the similar laws according to the reference. We randomly sampled 90 points in remote sensing images, the average, maximum and minimum of NDVI were calculated, and results can be seen in the following Fig. 3: (1) In aggregate, the NDVI values of bright vegetation area are the highest, fol-

lowed by shaded vegetation area, and water area is the lowest; (2) The difference of NDVI among different kinds of vegetation is not obvious. NDVI of the bright vegetation area is about 0.9, except for the shaded vegetation area of Landsat 7 ETM NDVI is 0.54, NDVI values are all above 0.7 in the other three remote sensing images; (3) The NDVI values in water area are the lowest, which is generally between 0.2 to 0.4; (4) By taking all sample values into account, there are also the phenomena of crossing in the NDVI of the three typical objects which are inclined to confuse features of bright vegetation area, shaded vegetation area and water area. A number of studies have shown that it is difficult to distinguish water, vegetation and other objects effectively in many cases with the only NDVI use[27-29]. Combining the above analysis, it is easy to understand that the main cause of confusion between water and vegetation is that the phenomena of "different objects are in the same spectrum" in water area and shaded vegetation area. The results may be the increase of water reflectivity and the decrease of vegetation reflectivity. For instance, when the flood disaster occurs, it will add sediment, suspension and impurity which will lead to the rising of reflectivity[30-32]. The existence of shadows will also result in the loss of spectral information.

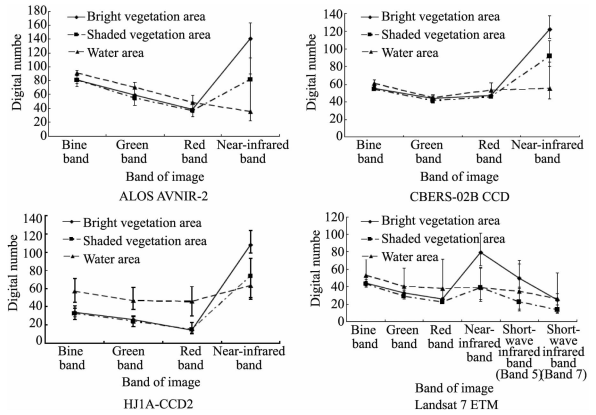


Fig. 2　Statistics of DN in bright vegetation area, shaded vegetation area and water area

图 2　明亮区植被、阴影区植被、水体区 DN 值统计

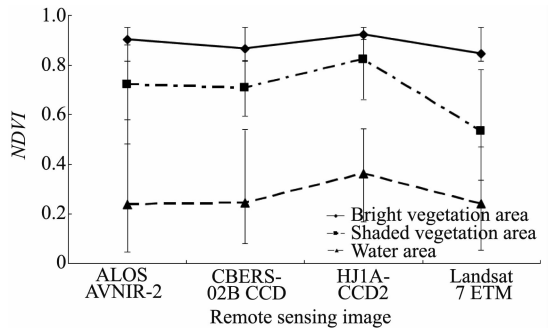


Fig. 3　Statistics of NDVI in bright vegetation area, shaded vegetation area and water area

图 3　明亮区植被、阴影区植被、水体区 NDVI 值统计

### 2.2　Constructing algorithm of NSVI

The above analyses show that there is crossing in each graph of visible band, near-infrared band, NDVI and the phenomena "different objects are in the same spectrum" lead to the misclassification. But there is obvious difference in near-infrared band of bright vegetation area, shaded vegetation area and water area. The DN value of bright vegetation ranks the first, then shaded vegetation is the second and the water area is the lowest. Because NDVI is one of indicators for features, it can magnify the difference among the three objects and make easier distinguishing by multiplying the value of NDVI and the value of near-infrared band. Therefore, it constructed a model of Shaded Vegetation Index (SVI) and its formula is:

$$\mathrm{SVI} = \mathrm{NDVI} \times \mathrm{NIR} = \frac{(\mathrm{NIR} - \mathrm{R}) \times \mathrm{NIR}}{\mathrm{NIR} + R} \quad , \quad (1)$$

where SVI is Shaded Vegetation Index; NDVI is Normalized Difference Vegetation Index; NIR is the grey value of near-infrared band; and $R$ is the gray value of red band.

The DN of original pixels in remote sensing images is in [0, 255], while NDVI was normalized in the rage of [0, 1]. So it is evident that SVI can enlarge the absolute difference between the ground and object which will be further proved in the following paragraphs. Because the relative difference is more valuable than absolute difference, the relative difference $I$ is defined as:

$$I = \frac{V - V_{\min}}{V_{\min}} \quad , \quad (2)$$

where $I$ represents the relative difference between the original target ground object and the target ground object with minimal value of DN or NDVI; $V$ represents the value of DN or NDVI of the target ground object; $V_{\min}$ represents the minimal value of DN or NDVI.

In order to maintain the same level with NDVI, SVI was normalized which turned to normalized shaded vegetation index and the formula is:

$$\mathrm{NSVI} = \frac{\mathrm{SVI} - \mathrm{SVI}_{\min}}{\mathrm{SVI}_{\max} - \mathrm{SVI}_{\min}} \quad , \quad (3)$$

where NSVI is normalized shaded vegetation index; $\mathrm{SVI}_{\max}$ is the maximum of SVI and $\mathrm{SVI}_{\min}$ is the minimum of SVI in the corresponding range.

## 3　Application effects of NSVI

### 3.1　Evaluation of enhancement effect on spectral difference

As the normalized vegetation index, the calculation of NSVI needs to use the maximum and minimum of NSVI within the range. In our research, $\mathrm{NSVI}_{\max}$ and $\mathrm{NSVI}_{\min}$ were adopted from two perspectives. First, the relative values of difference $I_{\mathrm{NSVI}p}$ of bright vegetation area, shaded vegetation area and water area were calculated respectively, based on 90 random sample points. Second, it calculated the relative difference $I_{\mathrm{NSVI}t}$ on the basis of whole experimental remote sensing images. The results in Table 2 are as follows: (1) The features of the normalized mean value of NIR is that the bright vegetation is on the top, then followed by shaded vegetation area and the last is water area. But, the relative difference between shaded vegetation area and water area is not significant according to the data from HJ1A-CCD2

and Landsat 7 ETM. (2) The means of NDVI have the same features, but the relative difference of NDVI is higher than the normalized NIR. The relative difference between shaded vegetation area and water area is enlarged, but there is a declining trend of the relative difference between bright vegetation area and shaded vegetation area which is related to the "saturation" problem of NDVI. (3) It shows a clear rank of the NSVI means of three ground objects which enlarges the difference between bright vegetation area and shaded vegetation area as well as shaded vegetation area and water area, and it can also provide an important reference for solving the "saturation" problem of NDVI. Obviously, NSVI has enlarged the difference among bright vegetation area, shaded vegetation area and water area which can provide a new method for the effective shadow detection of remote sensing images.

### 3.2 Analysis on classification effect

Through the above analyses, it can be drawn that NSVI can not only ensure the absolute difference among bright vegetation area, shaded vegetation area and water area, but also substantially enlarge the relative difference. Due to the magnified difference, it helps to get a better classification effect. With the reference to principle of object recognition, the thresholds of NSVI were determined combined with the accuracy of random verification point and the visual effect. The setting of threshold has direct influence on the image classification. Therefore, it took 0.01 as step to calculate the classification accuracy successively on the basis of ascertained threshold intervals, and the highest one is the setting threshold. NSVI thresholds of four remote sensing images are shown in Table 3, and the classification results in Fig. 4. Accuracy assessment method was adopted in the classification. In each image, 300 verification points were generated randomly. Table 4 indicates that overall classification accuracy is over 97%, and the overall Kappa coefficient is above 0.96. The detection accuracy of shaded vegetation area is above 94% and the Kappa coefficient is higher than 0.96 which correspond to the previous point. Likewise, three vegetation indices of NDVI, normalized difference umbra index (NDUI)[33] and shadow index (SI)[34] were introduced to evaluate the classification accuracy. Table 5 shows that NDVI is able to distinguish vegetation and water information but fails to distinguish bright vegetation area and shadow vegetation area effectively. The classification effect of SI is better than NDUI but neither can be compared with that of NSVI.

**Table 3 Threshold setting of bright vegetation area, shaded vegetation area and water area**

**表3 明亮区植被、阴影区植被、水体区阈值设定**

| Object \ Image type | ALOS AVNIR-2 | CBERS-02B CCD | HJ1A-CCD2 | Landsat 7 ETM |
|---|---|---|---|---|
| Bright vegetation area | NSVI≥0.46 | NSVI≥0.58 | NSVI≥0.60 | NSVI≥0.50 |
| Shaded vegetation area | 0.09<NSVI<0.46 | 0.23<NSVI<0.58 | 0.31<NSVI<0.60 | 0.11<NSVI<0.50 |
| Water area | NSVI≤0.09 | NSVI≤0.23 | NSVI≤0.31 | NSVI≤0.11 |

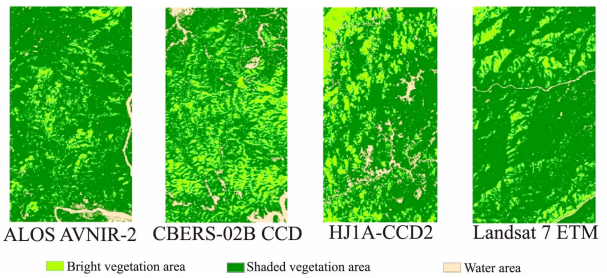


图4 试验影像分类结果

Fig. 4 Classification results of experimental images

There may be a misclassification among bright vegetation area, shaded vegetation area and water area, for example, the shaded vegetation area may be classified by mistake as water area and vice versa. According to the construction principle of NSVI and the classification of sample points, the spectral features of several sample points which are still misclassified were analyzed emphatically, then it can be seen that for the sample points which are close to the threshold of NSVI classification, if the value of near-infrared band is higher and NDVI is lower or NDVI is higher and near-infrared band is lower in one of two ground objects, there still is the possibility of misclassification. Of course, the probability will decrease substantially in contrast to NDVI.

**Table 2 Enhancement effect on spectral difference in NSVI**

**表2 NSVI光谱差异增强效果**

| Image type | Object | Normalized NIR mean | NDVI mean | NSVI mean | $I_{NIR}$ | $I_{NDVI}$ | $I_{NSVIp}$ | $I_{NSVIt}$ |
|---|---|---|---|---|---|---|---|---|
| ALOS AVNIR-2 | Bright vegetation area | 0.55 | 0.90 | 0.83 | 2.93 | 2.77 | 11.12 | 12.40 |
| | Shaded vegetation area | 0.32 | 0.72 | 0.39 | 1.29 | 2.02 | 4.81 | 5.36 |
| | Water area | 0.14 | 0.24 | 0.06 | – | – | – | – |
| CBERS-02B CCD | Bright vegetation area | 0.48 | 0.87 | 0.85 | 1.22 | 2.51 | 6.08 | 7.92 |
| | Shaded vegetation area | 0.36 | 0.71 | 0.51 | 0.66 | 1.87 | 3.39 | 4.41 |
| | Water area | 0.22 | 0.25 | 0.09 | – | – | – | – |
| HJ1A-CCD2 | Bright vegetation area | 0.42 | 0.92 | 0.85 | 0.72 | 1.54 | 3.29 | 5.12 |
| | Shaded vegetation area | 0.29 | 0.82 | 0.49 | 0.17 | 1.26 | 1.61 | 2.51 |
| | Water area | 0.25 | 0.36 | 0.14 | – | – | – | – |
| Landsat 7 ETM | Bright vegetation area | 0.31 | 0.85 | 0.72 | 1.06 | 2.52 | 5.82 | 6.97 |
| | Shaded vegetation area | 0.15 | 0.54 | 0.22 | 0 | 1.23 | 1.19 | 1.42 |
| | Water area | 0.15 | 0.24 | 0.09 | – | – | – | – |

**Table 4　Accuracy assessment of classification results based on NSVI**

**表 4　基于 NSVI 的分类结果精度评估**

ALOS AVNIR-2

| Class name | Reference totals | Classified totals | Number correct | Producers accuracy/% | Users accuracy/% | Kappa coefficient |
|---|---|---|---|---|---|---|
| Bright vegetation area | 100 | 103 | 100 | 100 | 99.01 | 0.985 1 |
| Shaded vegetation area | 100 | 96 | 95 | 95.00 | 98.96 | 0.984 4 |
| Water area | 100 | 103 | 99 | 99.00 | 96.12 | 0.941 7 |
| Overall classification accuracy = 98.00%　Overall Kappa coefficient = 0.970 0 | | | | | | |

CBERS-02B CCD

| Class name | Reference totals | Classified totals | Number correct | Producers accuracy/% | Users accuracy/% | Kappa coefficient |
|---|---|---|---|---|---|---|
| Bright vegetation area | 100 | 101 | 100 | 100 | 99.01 | 0.985 1 |
| Shaded vegetation area | 100 | 96 | 94 | 94.00 | 97.92 | 0.968 8 |
| Water area | 100 | 103 | 98 | 98.00 | 95.15 | 0.927 2 |
| Overall classification accuracy = 97.33%　Overall Kappa coefficient = 0.960 0 | | | | | | |

HJ1A-CCD2

| Class name | Reference totals | Classified totals | Number correct | Producers accuracy/% | Users accuracy/% | Kappa coefficient |
|---|---|---|---|---|---|---|
| Bright vegetation area | 100 | 100 | 100 | 100 | 100 | 1 |
| Shaded vegetation area | 100 | 103 | 98 | 98.00 | 95.15 | 0.969 1 |
| Water area | 100 | 97 | 95 | 95.00 | 97.94 | 0.927 2 |
| Overall classification accuracy = 97.67%　Overall Kappa coefficient = 0.965 0 | | | | | | |

Landsat 7 ETM

| Class name | Reference totals | Classified totals | Number correct | Producers accuracy/% | Users accuracy/% | Kappa coefficient |
|---|---|---|---|---|---|---|
| Bright vegetation area | 100 | 100 | 100 | 100 | 100 | 1 |
| Shaded vegetation area | 100 | 101 | 99 | 99.00 | 98.02 | 0.970 3 |
| Water area | 100 | 99 | 98 | 98.00 | 98.99 | 0.984 8 |
| Overall classification accuracy = 99.00%　Overall Kappa coefficient = 0.985 0 | | | | | | |

**Table 5　Accuracy assessment of classification results based on NDVI, NDUI, SI**

**表 5　基于 NDVI、NDUI、SI 的分类结果精度评估**

ALOS AVNIR-2

| Vegetation index | Class name | Reference totals | Classified totals | Number correct | Producers accuracy/% | Users accuracy/% | Kappa coefficient |
|---|---|---|---|---|---|---|---|
| NDVI | Bright vegetation area | 100 | 97 | 54 | 54.00 | 55.67 | 0.326 7 |
| | Shaded vegetation area | 100 | 100 | 53 | 53.00 | 53.00 | 0.300 3 |
| | Water area | 100 | 102 | 98 | 98.00 | 96.08 | 0.948 3 |
| | Overall classification accuracy = 68.33%　Overall Kappa coefficient = 0.528 4 | | | | | | |
| NDUI | Bright vegetation area | 100 | 88 | 60 | 60.00 | 68.18 | 0.474 2 |
| | Shaded vegetation area | 100 | 93 | 59 | 59.00 | 63.44 | 0.427 5 |
| | Water area | 100 | 119 | 89 | 89.00 | 74.79 | 0.706 4 |
| | Overall classification accuracy = 69.33%　Overall Kappa coefficient = 0.540 0 | | | | | | |
| SI | Bright vegetation area | 100 | 112 | 89 | 89.00 | 79.46 | 0.708 2 |
| | Shaded vegetation area | 100 | 87 | 71 | 71.00 | 81.61 | 0.651 2 |
| | Water area | 100 | 101 | 81 | 81.00 | 80.20 | 0.752 4 |
| | Overall classification accuracy = 80.33%　Overall Kappa coefficient = 0.705 0 | | | | | | |

CBERS-02B CCD

| Vegetation index | Class name | Reference totals | Classified totals | Number correct | Producers accuracy/% | Users accuracy/% | Kappa coefficient |
|---|---|---|---|---|---|---|---|
| NDVI | Bright vegetation area | 100 | 104 | 61 | 61.00 | 58.65 | 0.391 1 |
| | Shaded vegetation area | 100 | 94 | 53 | 53.00 | 56.38 | 0.330 0 |
| | Water area | 100 | 102 | 98 | 98.00 | 96.08 | 0.955 2 |
| | Overall classification accuracy = 70.67%　Overall Kappa coefficient = 0.560 0 | | | | | | |
| NDUI | Bright vegetation area | 100 | 95 | 68 | 68.00 | 71.58 | 0.551 9 |
| | Shaded vegetation area | 100 | 85 | 59 | 59.00 | 69.41 | 0.477 9 |
| | Water area | 100 | 120 | 90 | 90.00 | 75.00 | 0.714 3 |
| | Overall classification accuracy = 72.33%　Overall Kappa coefficient = 0.585 0 | | | | | | |

| Vegetation index | Class name | Reference totals | Classified totals | Number correct | Producers accuracy/% | Users accuracy/% | Kappa coefficient |
|---|---|---|---|---|---|---|---|
| SI | Bright vegetation area | 100 | 99 | 78 | 78.00 | 78.79 | 0.6767 |
| | Shaded vegetation area | 100 | 93 | 70 | 70.00 | 75.27 | 0.5954 |
| | Water area | 100 | 108 | 88 | 88.00 | 81.48 | 0.7647 |
| | Overall classification accuracy = 78.67% | | | Overall Kappa coefficient = 0.6800 | | | |

HJ1A-CCD2

| Vegetation index | Class name | Reference totals | Classified totals | Number correct | Producers accuracy/% | Users accuracy/% | Kappa coefficient |
|---|---|---|---|---|---|---|---|
| NDVI | Bright vegetation area | 100 | 104 | 60 | 60.00 | 57.69 | 0.3762 |
| | Shaded vegetation area | 100 | 94 | 52 | 52.00 | 55.32 | 0.3147 |
| | Water area | 100 | 102 | 98 | 98.00 | 96.08 | 0.9552 |
| | Overall classification accuracy = 70.00% | | | Overall Kappa coefficient = 0.5500 | | | |
| NDUI | Bright vegetation area | 100 | 118 | 81 | 81.00 | 68.64 | 0.5981 |
| | Shaded vegetation area | 100 | 80 | 60 | 60.00 | 75.00 | 0.5263 |
| | Water area | 100 | 102 | 78 | 78.00 | 76.47 | 0.6567 |
| | Overall classification accuracy = 73.00% | | | Overall Kappa coefficient = 0.5950 | | | |
| SI | Bright vegetation area | 100 | 111 | 88 | 88.00 | 79.28 | 0.7445 |
| | Shaded vegetation area | 100 | 91 | 75 | 75.00 | 79.28 | 0.6854 |
| | Water area | 100 | 98 | 80 | 80.00 | 81.63 | 0.7136 |
| | Overall classification accuracy = 81.00% | | | Overall Kappa coefficient = 0.7150 | | | |

Landsat 7 ETM

| Vegetation index | Class name | Reference totals | Classified totals | Number correct | Producers accuracy/% | Users accuracy/% | Kappa coefficient |
|---|---|---|---|---|---|---|---|
| NDVI | Bright vegetation area | 100 | 103 | 66 | 66.00 | 64.08 | 0.4715 |
| | Shaded vegetation area | 100 | 97 | 60 | 60.00 | 61.86 | 0.4181 |
| | Water area | 100 | 100 | 97 | 97.00 | 97.00 | 0.9550 |
| | Overall classification accuracy = 74.33% | | | Overall Kappa coefficient = 0.6150 | | | |
| NDUI | Bright vegetation area | 100 | 101 | 80 | 80.00 | 79.21 | 0.6933 |
| | Shaded vegetation area | 100 | 101 | 78 | 78.00 | 77.23 | 0.6633 |
| | Water area | 100 | 98 | 77 | 77.00 | 78.57 | 0.6682 |
| | Overall classification accuracy = 78.33% | | | Overall Kappa coefficient = 0.6750 | | | |
| SI | Bright vegetation area | 100 | 102 | 84 | 84.00 | 82.35 | 0.7463 |
| | Shaded vegetation area | 100 | 100 | 79 | 79.00 | 79.00 | 0.6850 |
| | Water area | 100 | 98 | 82 | 82.00 | 83.67 | 0.7437 |
| | Overall classification accuracy = 81.67% | | | Overall Kappa coefficient = 0.7250 | | | |

## 4 Discussion

### 4.1 Physical significance of NSVI and applicability

The construction of NSVI is based on NDVI with the use of radiation difference of near-infrared band. It not only solves the problem that NDVI can only weaken part of topographic influence, but also enlarges the spectral difference between ground objects, so as to particularly improve the validity of shadow detection. From the process of the index construction, this index model is suitable for the near-infrared band where there is a significant difference, but its application is far from limited in these three objects in this study. The experimental images are from different sensors under different space, time and spectral resolution. The results show that NSVI is universal to optical images. With the development of remote sensing technology and the constant improvement of each quality indicators, the spectral enhancement effect and mechanism of NSVI can still be applied into further exploration and research.

### 4.2 Analysis on image histogram features

According to the respective statistical histograms of NDVI and NSVI which are based on the data of ALOS AVNIR-2, CBERS-02B CCD, HJ1A-CCD2 and Landsat 7 ETM, four remote sensing images (Fig. 5), it can be seen that there is an obvious distribution deflecting to left in each NDVI histogram, while NSVI histograms can better solve the problem of the skewed distribution and make the image histograms closer to the normal distribution which is more accordant with practical circumstances and provides convenience for the interpretation of remote sensing images. All of mean values of NDVI that are above 0.65, the large ratio of high value and the right skewed peak of frequency distribution are the compelling evidences for the "saturation" problem of NDVI, while NSVI can overcome the above problems by the virtue of enlarging spectral difference.

### 4.3 Verification for shadow removal feasibility

Although the spectral response of shaded vegetation is weaker than that of bright vegetation area, it still has the basic spectral features of vegetation. Assuming that there are two pixels of which elevation, slope, position, aspect and other topographic factors are all similar and

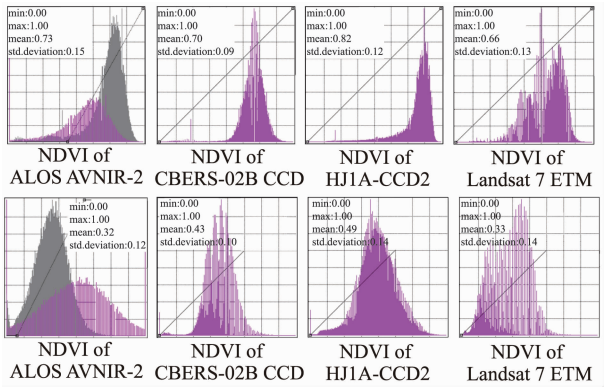


Fig. 5　NDVI and NSVI histograms of experimental images
图 5　试验影像 NDVI、NSVI 直方图

the types of aboveground vegetation is close to coverage, then the spectral values of these two pixels are approximately equal in theory. If the slope aspect of one pixel is different, the spectral value in shaded vegetation area will decrease. Therefore, the pixel value of shaded vegetation area will be corrected as bright vegetation area which is the main work on shadow removal and information restoration. Many methods for shadow removal of remote sensing images have been proposed in previous studies. This study only demonstrates the feasibility of effective shadow detection, shadow removal and the spectral information restoration in shaded vegetation area with NSVI. The typical spectral matching method was adopted in this study. Took the image of ALOS AVNIR-2 as an example, and 80 pixels (40 pairs) with similar properties on both sides of the same ridge and valley were selected to record the band values of bight vegetation area and shaded vegetation area (Fig. 6). After the undetermined coefficients were calculated, the obtained formula is as follows:

$$B_b = aB_s + b \quad , \quad (4)$$

where $B_b$ is the grayscale of band in bright area; $B_s$ is the grayscale of band in shaded area; $a$ and $b$ are undetermined coefficients.

Figure 7 shows that in four bands of ALOS AVNIR-2 image, $R^2$ in spectral matching model of bright vegetation area and shaded vegetation area is above 0.5, $P$ = 0.0000, reaching an extremely significant level which forms a good match. It proves the feasibility of converting the spectrum of shaded vegetation area to that of bright vegetation area through the model and also further confirms the ability of constructed normalized shaded vegetation index (NSVI) on shadow detection of remote sensing images.

## 5　Conclusions

Shadow is the vital cause of the phenomena that "the same object has different spectra" and "the different objects are in the same spectrum" in remote sensing images, resulting in serious loss of ground object information and greatly affecting target object recognition and image segmentation which restrict the application of remote sensing technique in resource, environment, society, economy and other fields. The purpose of this research is to explore an effective shadow detection method for images and evaluate its application effects by constructing the model of Normalized Shaded Vegetation Index (NSVI).

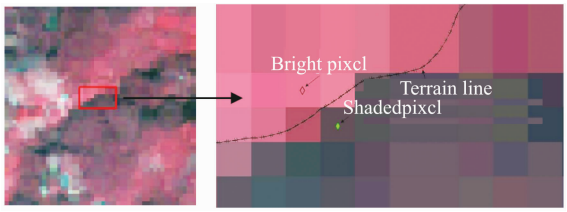


Fig. 6　Sketches of the bright vegetation and shaded vegetation pixels on both sides of terrain line
图 6　地形线两侧明亮区植被、阴影区植被像元示意图

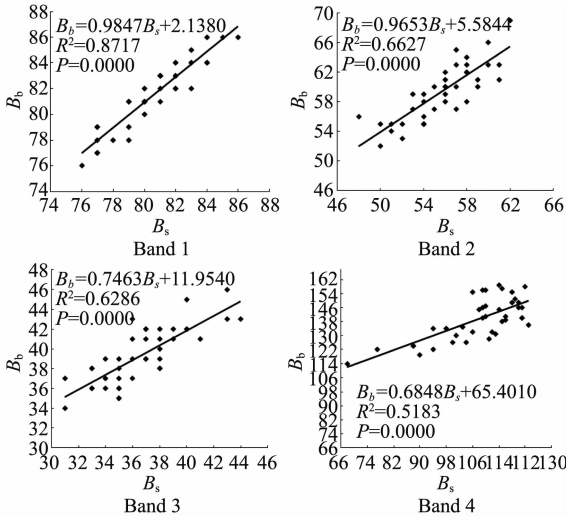


Fig. 7　Relationships of spectral matching between bright vegetation area and shaded vegetation area of ALOS AVNIR-2 image
图 7　ALOS AVNIR-2 影像明亮区植被、阴影区植被光谱匹配关系

(1) By comparing the mean values of near-infrared band, NDVI and NSVI in bright vegetation area, shaded vegetation area, water area, it can be concluded that *NSVI* has substantially enlarged the spectral difference among three objects and takes on a clear relationship of their values.

(2) NSVI threshold method was adopted to classify the experimental images. The results show that the overall classification accuracy of each image is above 97% and overall Kappa coefficient is above 0.96. It also has an excellent accuracy in shaded vegetation area.

(3) NSVI histogram is close to the normal distribution which is more appropriate for objects without "saturation" problem of NDVI. In this study, NSVI is constructed with intuitive physical meaning whose good shadow detection ability will provide a feasible approach to shadow removal and information restoration in remote sensing images.

## References


[1] Kantsingh K, Pal K J, Nigam M. Shadow detection and removal from remote sensing images using NDI and morphological operators[J]. *International Journal of Computer Applications*, 2012, **42**(10): 37-40.

[2] Zhang H, Sun K, Li W. Object-oriented shadow detection and removal from urban high-resolution remote sensing images[J]. *IEEE Transactions on Geoscience & Remote Sensing*, 2014, **52**(11): 6972-6982.

[3] Anoopa S, Dhanya V, Kizhakkethottam J J. Shadow detection and removal using tri-class based thresholding and shadow matting technique [J]. *Procedia Technology*, 2016, **24**: 1358-1365.

[4] Ambrosio G. Shadow detection in colour high-resolution satellite images[J]. *International Journal of Remote Sensing*, 2008, **29**(7): 1945-1963.

[5] Chung K L, Lin Y R, Huang Y H. Efficient shadow detection of color aerial images based on successive thresholding scheme [J]. *IEEE Transactions on Geoscience & Remote Sensing*, 2009, **47**(2): 671-682.

[6] Liasis G, Stavrou S. Satellite images analysis for shadow detection and building height estimation[J]. *ISPRS Journal of Photogrammetry & Remote Sensing*, 2016, **119**: 437-450.

[7] Li Y, Gong P, Sasagawa T. Integrated shadow removal based on photogrammetry and image analysis[J]. *International Journal of Remote Sensing*, 2005, **26**(18): 3911-3929.

[8] Yang J, Zhao Z M, Yang J. Shadow removal method for high resolution remote sensing image[J]. Geomatics and Information Science of Wuhan University, 2008, **33**(1): 17-20.

[9] Yamazaki F, Liu W, Takasaki, M. Characteristics of shadow and removal of its effects for remote sensing imagery[J]. *IEEE International Geoscience and Remote Sensing Symposium*, *IGARSS*, 2009, **4**: 426-429.

[10] Zigh E, Belbachir M F, Kadiri M, *et al*. New shadow detection and removal approach to improve neural stereo correspondence of dense urban VHR remote sensing images[J]. *European Journal of Remote Sensing*, **48**: 447-463.

[11] Su N, Zhang Y, Tian S, *et al*. Shadow detection and removal for occluded object information recovery in urban high-resolution panchromatic satellite images[J]. *IEEE Journal of Selected Topics in Applied Earth Observations & Remote Sensing*, **9**(6): 2568-2582.

[12] Yan L, Sasagawa T, Peng G, A system of the shadow detection and shadow removal for high resolution city aerial photo[J]. *Xxth ISPRS Congress*, 2004, Istanbul, Jul. 12-23.

[13] Li R, Zhang B, Zhang X, et al. Practical method of shadow detection and removal for high spatial resolution remote sensing image[C]. *MIPPR* 2007: *Remote Sensing and GIS Data Processing and Applications*; *and Innovative Multispectral Technology and Applications*, Wuhan, 2007, Nov. 15, p. 67900Q

[14] Zhi P U, Liao Y, Jie B. Shadow detection and removal based on object-oriented method in high spatial resolution remote sense image[J]. *Remote Sensing Technology & Application*. 2008, **23**(6): 735-738.

[15] Li B, Zhang H, Xu F. Water extraction in high resolution remote sensing image based on hierarchical spectrum and shape features[C]. 35$^{th}$ *International Symposium on Remote Sensing of Environment* (*ISRSE*35), Beijing, 2014, Apr. 22-26, 17, p. 1-6.

[16] Petus C, Lewis M, White D. Monitoring temporal dynamics of great artesian basin wetland vegetation, Australia, using MODIS NDVI[J]. *Ecological Indicators*, 2013, **34**(11): 41-52.

[17] Qiao T, Zhang H Q, Chen Y F, *et al*. Extraction of vegetation information based on NDVI segmentation and object-oriented method[J]. *Journal of Northwest Forestry University*, 2013, **59**(4): 328-333.

[18] Fleming S W, Lavenue A M, Aly A H. Practical applications of spectral analysis to hydrologic time series[J]. *Hydrological Processes*, 2002, **16**(2): 565-574.

[19] Schaefli B, Maraun D, Holschneider M. What drives high flow events in the Swiss Alps? Recent developments in wavelet spectral analysis and their application to hydrology. Advances in Water *Resources*, 2007, **30**(12): 2511-2525.

[20] Aneglini P. Correlation and spectral analysis of two hydrogeological systems in central Italy[J]. *Hydrological Sciences Journal*, 2009, **42**(3): 425-438.

[21] Han X Y, Han L, Chen L W. Extraction of vegetation information using adding windows *DTW* distance with NDVI time series data[J]. *Engineering of Surveying & Mapping*, 2016, **25**(3): 11-16.

[22] Liu Y, Guo Y, Wang J, *et al*. A preliminary approach on the synchronically ground based measurement of spectral reflectance, NDVI, LAI, and the temperature and moisture of soils[J]. *Proceedings of SPIE - The International Society for Optical Engineering*, 7123, Beijing, Nov. 24, pp. 712310-1-712310-7.

[23] Prakash K L, Raghavendra K, Somashekar R K. Temporal-scale spectral variability analysis of water quality parameters to realize seasonal behaviour of a tropical river system-River Cauvery, India[J]. *Journal of Environmental Biology*, 2009, **30**: 235-240.

[24] Santin-Janin H, Garel M, Chapuis J L, *et al*. Assessing the performance of NDVI as a proxy for plant biomass using non-linear models: a case study on the Kerguelen archipelago[J]. Polar Biology, 2009, **32**(6): 861-871.

[25] Fang Q M, Zhan Z M. A novel dynamic stretching solution to eliminate saturation effect in NDVI and its application in drought monitoring [J]. *Chinese Geographical Science*, 2012, **22**(6): 683-694.

[26] Gu Y, Wylie B K, Howard D M, *et al*. NDVI saturation adjustment: a new approach for improving cropland performance estimates in the Greater Platte River Basin, USA[J]. Ecological Indicators, 2013, **30**(2): 1-6.

[27] Liu P, Zhang Y, Zhou B, *et al*. Land use/cover classification using multi-source data with SAM. Journal of Zhejiang University (Engineering Science), 2009, **43**(9): 1574-1579.

[28] Babal M, Daniska J, Mikus J, *et al*. Modelling index of thermophily by means of a multi-source database on Broggerhalvoya Peninsula (Svalbard)[J]. International Journal of Remote Sensing, 2010, **23**(21): 4683-4698.

[29] Creech T G, Epps C W, Monello R J, *et al*. Predicting diet quality and genetic diversity of a desert-adapted ungulate with NDVI[J]. *Journal of Arid Environment*, 2016, **127**: 160-170.

[30] Rudorff C M, Galv? o L S, Novo E M L M. Reflectance of floodplain waterbodies using EO-1 Hyperion data from high and receding flood periods of the Amazon river. International Journal of Remote Sensing, 2013, **30**(10): 2713-2720.

[31] Kanungo D P, Sarkar S. Use of multi-source data sets for land use/land cover classification in a hilly terrain for landslide study[J]. *Disaster & Development*, 2011, **5**(1): 35-51.

[32] Legout C, Poulenard J, Nemery J, *et al*. Quantifying suspended sediment sources during flood events in headwater catchments using diffuse reflectance spectroscopy[C]. *EGU General Assembly*, *Vienna*, 2013, Apr. 7-12, p. 15.

[33] Zhou J H, Zhou Y F, Guo X H, *et al*. Methods of extracting distribution information of plants at urban darken areas and repairing their brightness[J]. *Journal of East China Normal University* (*Natural Science*), 2011, **6**: 1-9.

[34] Liu H, Xie T W. Study on shadow detection in high resolution remote sensing image based on PCA and HIS model[J]. *Remote Sensing Technology and Application*, 2013, **28**(1): 78-84.

[35] Legout C, Poulenard J, Nemery J, *et al*. Quantifying suspended sediment sources during flood events in headwater catchments using diffuse reflectance spectroscopy[C]. *EGU General Assembly*, *Vienna*, 2013, Apr. 7-12, p. 15.

[36] Zhou J H, Zhou Y F, Guo X H, *et al*. Methods of extracting distribution information of plants at urban darken areas and repairing their brightness[J]. *Journal of East China Normal University* (*Natural Science*), 2011, **6**: 1-9.

[37] Liu H, Xie T W. Study on shadow detection in high resolution remote sensing image based on PCA and HIS model[J]. *Remote Sensing Technology and Application*, 2013, **28**(1): 78-84.